Conductance between two STM probes in carbon nanotubes

Takeshi NAKANISHI and Tsuneya ANDO[1]

Research Center for Advanced Carbon Materials, AIST
1–1–1 Higashi, Tsukuba 305-8565, Japan

[1] *Department of Physics, Tokyo Institute of Technology*
2–12–1 Ookayama, Meguro-ku, Tokyo 152-8551, Japan

The conductance image between two probes of scanning-tunneling-microscopy (STM) is calculated in an armchair carbon nanotube within a tight-binding model and a realistic model for STM probes. A Kekulé-type pattern usually appears due to interference of states at K and K' points except in special cases.

Keywords: graphite, carbon nanotube, fullerene tube, STM, recursive Green's function technique

§1. Introduction

Carbon nanotubes are regarded as ballistic conductors. In metallic nanotubes, in particular, the backward scattering is entirely suppressed for scatterers with potential range larger than the lattice constant of a two-dimensional graphite and the conductance is quantized into $2e^2/\pi\hbar$.[1–3] When several bands are occupied, a perfectly conducting channel transmitting through the system without being scattered back is present.[4] It is known that scanning tunneling microscopy (STM) and spectroscopy (STS) are a powerful technique for directly viewing electronic wave functions at the atomic level. Quite recently multi-probe STM was developed.[5–14] In this paper, we calculate two-probe STM image to explicitly visualize interference effects in ballistic carbon nanotubes.

STM measurements have been conducted to observe the electronic wavefunctions in carbon nanotubes.[15,16] Energy-dependent interference patterns in the wavefunctions were observed in nanotubes shortened to less than 40 nm.[16] Numerical calculations were made on electronic states and STM images in a finite carbon nanotube.[17,18] Topographical STM images have been calculated within a tight-binding model and the appearance of the honeycomb structure has been demonstrated in infinitely long nanotubes.[19,20] The tight-binding calculation has been applied to investigate native defects in carbon nanotubes,[21] and effects of tip shape.[22] Orbital magnetic moments were shown to be induced in carbon nanotubes placed between STM probes.[23]

In this work, we shall calculate the conductance between two STM probes in carbon nanotubes and demonstrate the importance of interference effects. In §2, a model and method of calculation are discussed together with a realistic model of STM probes, and the appearance and disappearance of interference patters due to the presence of K and K' points are discussed. Numerical results are presented in §3. A discussion and summary are given in §4.

§2. Formulation

2.1 Preliminaries

Figure 1 (a) shows the structure of two–dimensional (2D) graphite or graphene, two primitive translation vectors $\boldsymbol{a}$ and $\boldsymbol{b}$, and three vectors $\vec{\tau}_l$ $(l=1,2,3)$ connecting nearest-neighbor atoms. A unit cell contains two carbon atoms denoted as A (open circle) and B (closed circle). The origin of the coordinates is chosen at a B site, i.e., a B site is given by $\boldsymbol{R}_B = n_a\boldsymbol{a}+n_b\boldsymbol{b}$ and an A site is $\boldsymbol{R}_A = n_a\boldsymbol{a}+n_b\boldsymbol{b}+\vec{\tau}$ with n_a and n_b being integers and $\vec{\tau}\equiv\vec{\tau}_1=(\boldsymbol{a}+2\boldsymbol{b})/3$. In the coordinate system (x', y') fixed onto the graphene sheet, we have $\boldsymbol{a} = a(1,\,0)$, $\boldsymbol{b}=a(1/2,\,\sqrt{3}/2)$, and $\vec{\tau}=a(0,\,1/\sqrt{3})$, where $a=0.246$ nm is the lattice constant. In the following we use a tight-binding model with a nearest-neighbor hopping integral $-\gamma_0$.

In a 2D graphite, two bands having approximately a linear dispersion cross the Fermi level at corner K and K' points of the first Brillouin zone. The wave vectors of the K and K' points are given by $\boldsymbol{K}=(2\pi/a)(1/3,\,1/\sqrt{3})$ and $\boldsymbol{K'}=(2\pi/a)(2/3,\,0)$. For states in the vicinity of the Fermi level $\varepsilon=0$, the wavefunction is written as[24]

$$\begin{aligned}\psi_A(\boldsymbol{R}_A) &= \mathrm{e}^{\mathrm{i}\boldsymbol{K}\cdot\boldsymbol{R}_A}F_A^K(\boldsymbol{R}_A)+\mathrm{e}^{\mathrm{i}\eta}\mathrm{e}^{\mathrm{i}\boldsymbol{K'}\cdot\boldsymbol{R}_A}F_A^{K'}(\boldsymbol{R}_A),\\ \psi_B(\boldsymbol{R}_B) &= -\omega\mathrm{e}^{\mathrm{i}\eta}\mathrm{e}^{\mathrm{i}\boldsymbol{K}\cdot\boldsymbol{R}_B}F_B^K(\boldsymbol{R}_B)+\mathrm{e}^{\mathrm{i}\boldsymbol{K'}\cdot\boldsymbol{R}_B}F_B^{K'}(\boldsymbol{R}_B),\end{aligned} \tag{2.1}$$

in terms of the slowly–varying envelope functions F_A^K, F_B^K, $F_A^{K'}$, and $F_B^{K'}$. Then, in the vicinity of the K point, for example, they satisfy the $\boldsymbol{k}\cdot\boldsymbol{p}$ equation:

$$\begin{aligned}&\gamma(\vec{\sigma}\cdot\hat{\boldsymbol{k}})\boldsymbol{F}^K(\boldsymbol{r})=\varepsilon\boldsymbol{F}^K(\boldsymbol{r}),\\ &\boldsymbol{F}^K(\boldsymbol{r})=\begin{pmatrix}F_A^K(\boldsymbol{r})\\ F_B^K(\boldsymbol{r})\end{pmatrix},\end{aligned} \tag{2.2}$$

where $\gamma=\sqrt{3}a\gamma_0/2$ is the band parameter, $\hat{\boldsymbol{k}}=(\hat{k}_x,\hat{k}_y)=-\mathrm{i}\vec{\nabla}$ is a wave vector operator, ε is the energy, and σ_x and σ_y are the Pauli spin matrices.

In nanotubes, the coordinate system (x, y) will be chosen in such a way that the x axis is in the chiral direction, *i.e.*, the direction along the circumference or the chiral vector $\boldsymbol{L}$, and the y axis in the direction of the axis. In metallic nanotubes, the $\boldsymbol{k}\cdot\boldsymbol{p}$ equation is solved under a periodic boundary condition in the x direction. The wave function for the linear bands at $\varepsilon=0$

is independent of the position and given by

$$\boldsymbol{F}^{K\pm}(\boldsymbol{r}) = \frac{1}{\sqrt{2LA}} \begin{pmatrix} \mp \mathrm{i} \\ 1 \end{pmatrix}, \tag{2.3}$$

$$\boldsymbol{F}^{K'\pm}(\boldsymbol{r}) = \frac{1}{\sqrt{2LA}} \begin{pmatrix} \pm \mathrm{i} \\ 1 \end{pmatrix}, \tag{2.4}$$

where $L=|\boldsymbol{L}|$, A is the length of the nanotube, and the upper and lower signs correspond to right and left-going waves, respectively.

2.2 Interference between K and K' Points

In this work, we consider an armchair nanotube with $\boldsymbol{L}=2n\boldsymbol{a}+n\boldsymbol{b}$ with integer n and chiral angle $\eta=-\pi/2$, which is metallic without depending on L. We consider the conductance between two STM tips in an infinitely long nanotube as illustrated in Fig. 1 (b). In this case, we have

$$\psi_A(\boldsymbol{R}_A) = \mathrm{e}^{\mathrm{i}\boldsymbol{K}\cdot\boldsymbol{R}_A} F_A^K(\boldsymbol{R}_A) - \mathrm{i}\,\mathrm{e}^{\mathrm{i}\boldsymbol{K}'\cdot\boldsymbol{R}_A} F_A^{K'}(\boldsymbol{R}_A), \tag{2.5}$$

$$\psi_B(\boldsymbol{R}_B) = \mathrm{i}\omega\,\mathrm{e}^{\mathrm{i}\boldsymbol{K}\cdot\boldsymbol{R}_B} F_B^K(\boldsymbol{R}_B) + \mathrm{e}^{\mathrm{i}\boldsymbol{K}'\cdot\boldsymbol{R}_B} F_B^{K'}(\boldsymbol{R}_B). \tag{2.6}$$

First, we consider traveling wave with $\varepsilon\approx 0$ injected from the B site $\boldsymbol{R}_B=0$. We may approximately take the lowest order of the coupling between the STM tip and carbon atoms, because the coupling is usually very weak. The injected electron equally propagates to both right and left directions, because of the symmetry of the configuration. Further, the wavefunction of the injected electron is decomposed into those at the K and K' point with the same amplitude. Then, eq. (2.6) shows that on the right hand side of the injection point $\boldsymbol{R}_B=0$, where the envelope functions become

$$\begin{aligned} \boldsymbol{F}^{K}(\boldsymbol{r}) &= -\mathrm{i}\omega^{-1}\delta\boldsymbol{F}^{K+}(\boldsymbol{r}), \\ \boldsymbol{F}^{K'}(\boldsymbol{r}) &= \delta\boldsymbol{F}^{K'+}(\boldsymbol{r}), \end{aligned} \tag{2.7}$$

with δ being the amplitude. Upon substitution of the above into eqs. (2.5) and (2.6), we have

$$\begin{aligned} \psi_A(\boldsymbol{R_A}) &= \frac{\delta}{\sqrt{2LA}}(\mathrm{e}^{\mathrm{i}\pi/3}\mathrm{e}^{\mathrm{i}\boldsymbol{K}\cdot\boldsymbol{R}_A}+\mathrm{e}^{\mathrm{i}\boldsymbol{K}'\cdot\boldsymbol{R}_A}), \\ &= \mathrm{i}\sqrt{\frac{2}{LA}}\delta\,\mathrm{e}^{\mathrm{i}\pi n_a}\sin\left[\frac{\pi}{3}(n_a-2n_b)\right], \\ \psi_B(\boldsymbol{R_B}) &= \frac{\delta}{\sqrt{2LA}}(\mathrm{e}^{\mathrm{i}\boldsymbol{K}\cdot\boldsymbol{R}_B}+\mathrm{e}^{\mathrm{i}\boldsymbol{K}'\cdot\boldsymbol{R}_B}). \\ &= \sqrt{\frac{2}{LA}}\delta\,\mathrm{e}^{\mathrm{i}\pi n_a}\cos\left[\frac{\pi}{3}(n_a-2n_b)\right]. \end{aligned} \tag{2.8}$$

The conductance between the STM probe at the origin and that at $\boldsymbol{R_B}$ is approximately proportional to the probability density $|\psi_B(\boldsymbol{R_B})|^2$. It becomes the maximum $\propto 2\delta^2$ for $n_a-2n_b=3m$ with an integer m and becomes $\propto(1/2)\delta^2$ for $n_a-2n_b=3m\pm1$. The probability density at A sites vanishes for n_a–$2n_b=3m$ and $\propto(3/2)\delta^2$ for $n_a-2n_b=3m\pm1$.

The sites $\tilde{\boldsymbol{R}}=n_a\boldsymbol{a}+n_b\boldsymbol{b}$ satisfying $n_a-2n_b=3m$ with integer m form a honeycomb lattice. Its basis vectors can be chosen as $\tilde{\boldsymbol{a}}=-\boldsymbol{a}-2\boldsymbol{b}$ and $\tilde{\boldsymbol{b}}=2\boldsymbol{a}+\boldsymbol{b}$ as shown in Fig. 1 (a), for example, and therefore the lattice constant is $\sqrt{3}a$ and the area of the unit cell is $3\Omega_0$ with $\Omega_0=(\sqrt{3}/2)a^2$ being the area of the original honeycomb lattice spanned by the basis vectors $\boldsymbol{a}$ and $\boldsymbol{b}$. The maximum conductance is observed when two STM probes couple to atoms on this enlarged lattice for both A and B sublattices. This Kekulé pattern is a result of the interference of traveling waves at the K and K' points as clearly shown in eq. (2.8). This so-called Kekulé pattern also appears in the wavefunction around a single vacancy[25] and a cap.[26]

Next we consider two interesting cases of injection through several atoms. It has been shown that the $\boldsymbol{k}\cdot\boldsymbol{p}$ equation has a special symmetry valid in metallic nanotubes.[27] We consider transformation Π defined as

$$\Pi : \begin{pmatrix} F_A^K(x,y) \\ F_B^K(x,y) \\ F_A^{K'}(x,y) \\ F_B^{K'}(x,y) \end{pmatrix} \to \begin{pmatrix} +\mathrm{i}F_B^K(-x,y) \\ -\mathrm{i}F_A^K(-x,y) \\ +\mathrm{i}F_B^{K'}(-x,y) \\ -\mathrm{i}F_A^{K'}(-x,y) \end{pmatrix}. \tag{2.9}$$

This operation Π commutes with the Hamiltonian and the boundary condition in metallic nanotubes. Because Π^2 is an identity, Π has eigenvalues $p=\pm1$, which is called parity. The physical meaning of this symmetry is clear in armchair nanotubes. The transformation Π is nothing but a mirror reflection around the y axis. In metallic nanotubes, the states are classified by the parity, i.e., $\boldsymbol{F}^{K+}$ and $\boldsymbol{F}^{K'-}$ have parity $p=-1$, while $\boldsymbol{F}^{K-}$ and $\boldsymbol{F}^{K'+}$ have parity $p=+1$.

It is possible in a special case to inject electron into one of the states with a parity. If a wave is injected from two neighbor sites at $\boldsymbol{R_B}$ and $\boldsymbol{R_B}+\vec{\tau}_1$ aligning in the circumference direction with the same amplitude, the injected symmetric state has the parity $p=+1$. Thus, the wave traveling in the positive y direction consists only of the K' point and that in the negative y direction consists only of the K point. As a result, there is no interference between the K and K' points and the resulting conductance does not exhibit a Kekulé pattern but that due to the original lattice.

On the other hand, the injection into the antisymmetric ($p=-1$) state is achieved, for examples, when the same waves are injected from a B site at $\boldsymbol{R}_B$ and two A sites at $\boldsymbol{R}_B+\vec{\tau}_2$ and $\boldsymbol{R}_B+\vec{\tau}_3$. In fact, because

$$-\gamma_0\sum_{l=1}^{3}\psi_A(\boldsymbol{R}_B+\vec{\tau}_l) = \varepsilon\psi_B(\boldsymbol{R}_B)\approx 0, \tag{2.10}$$

for $\varepsilon\approx 0$, the equal injection from these two A sites corresponds to the injection with opposite sign of the wavefunction from the A site at $\boldsymbol{R}_B+\vec{\tau}_1$. In this case, the wave traveling in the positive y direction consists only of the K point and that in the negative y direction consists only of the K' point. As a result, the conductance again does not exhibit a Kekulé pattern but that due to the original lattice. These features manifest themselves in the actual STM images shown in the next section.

2.3 Tip Model

Next, we consider a more realistic model of a nanotube with curvature and an STM tip with coupling to several carbon atoms. First, we assume that each π orbital is oriented in the direction perpendicular to the curved cylinder surface and possible lattice distortion

due to curvature is completely neglected. An STM tip is located on the surface of a cylinder with the same axis as the nanotube radius and with a fixed distance Δ. The STM tip is modeled by a chain of s-like atoms with nearest neighbor hopping integral $-t$ and the Fermi energy being fixed at the center of the one-dimensional band. An actual STM tip usually has a radius larger than the atomic distance and therefore the present model may be too simple. Effects associated with this complication will briefly be discussed in §5.

The hopping integral between the tip s atom and a π orbital at $\boldsymbol{R}$ of the tube is given by sp Slater–Koster form:[19,20]

$$t_{\boldsymbol{R}} = t_0 w_{\boldsymbol{R}} \exp\Big(-\frac{d_{\boldsymbol{R}}}{\lambda}\Big)\cos\theta_{\boldsymbol{R}},$$
$$w_{\boldsymbol{R}} = \exp(-\alpha^2 d_{\boldsymbol{R}}^2)\Big[\sum_{\boldsymbol{R}'}\exp(-\alpha^2 d_{\boldsymbol{R}'}^2)\Big]^{-1}, \qquad (2.11)$$

where $d_{\boldsymbol{R}}$ is the distance between the tip atom and the carbon atom, $\theta_{\boldsymbol{R}}$ is the angle with the orientation of the π orbital as shown in Fig. 1 (c). This model hopping integral with parameters $\lambda = 0.085$ nm, $\alpha^{-1} \approx 0.13$ nm, and $\Delta = 0.5$ nm has been introduced in previous works,[19,20] in which the asymmetry between A and B carbon atoms in multi-layer graphite[28] has successfully been reproduced. This hopping integral has a strong tendency to pick up contributions of carbon atoms lying closest to the tip because of the weight factor $w_{\boldsymbol{R}}$. The tip-sample coupling depends on the curvature of nanotubes and therefore the deviation from the hexagonal symmetry valid in 2D graphite is significant in the so-called (10,10) nanotube with $L/a = 10\sqrt{3}$ for which actual numerical calculations are performed.

In order to deal rigorously with the infinite nanotube, we solve numerically a scattering problem in a finite nanotube between two STM probes connected at both ends to semi-infinite nanotubes. We calculate the transmission probability between these two STM tips. In terms of the transmission probability T, the conductance G is given by $G=(e^2/\pi\hbar)T$ using the Landauer formula. In actual calculations we consider the so-called (10,10) nanotube with $L=10\sqrt{3}a$, and choose fixed parameters $t_0/\gamma_0=-10$, $t/\gamma_0=1$, and $\varepsilon=0$.

§3. Numerical Results

In the following, the left STM tip is fixed at several points on the lines shown in Fig. 2 and the right tip is continuously swept over the wide region. The actual coordinates of the left tip are given in Table I.

Figure 3 shows the conductance for varying the position of the right STM tip when the left tip is fixed at points 'a' to 'f' shown in Fig. 2. The position of the left tip is denoted by an open circle, but its actual position is shifted by $(0, -45)a$ in the coordinate system (x, y) shown in the Fig. 1 (a) and therefore is quite far from the right tip position. Because the distance between two tips is much larger than the circumference, the contribution only of traveling modes is dominant and therefore the conductance varies periodically in all the cases.

When the left tip is on top of site B_1 denoted by 'a' in Fig. 2, the conductance exhibits a clear Kekulé pattern and follows the simplified estimation presented in §2. In fact, the conductance is largest at B sites $\tilde{\boldsymbol{R}}_B$ related to the left-tip atom by the basis vectors $\tilde{\boldsymbol{a}}$ and $\tilde{\boldsymbol{b}}$. Further, it is the second largest at A sites $\tilde{\boldsymbol{R}_B}+\vec{\tau}_2$ and $\tilde{\boldsymbol{R}_B}+\vec{\tau}_3$, the third largest at B sites other than $\tilde{\boldsymbol{R}}_B$, and minimum at A sites $\tilde{\boldsymbol{R}_B}+\vec{\tau}_1$. With the increase in the displacement 'b' and 'c' corresponding to (b) and (c), respectively, this Kekulé pattern becomes weaker.

When the amount of the shift in the circumference x direction reaches $0.63\times a/\sqrt{3}$ as in Fig. 3 (d), the left tip couples almost equally to the B site at the origin and two of the neighboring A sites through $\vec{\tau}_2$ and $\vec{\tau}_3$. In this case, only the traveling wave with $p=-1$ is injected into $\boldsymbol{F}^{K+}$ and the Kekulé pattern disappears as has been mentioned in §2. Because the traveling wave is anti-symmetric between neighboring A and B sites along the circumference, the conductance vanishes when the right STM tip is located between them. Such destructive interference does not occur between neighboring A and B sites in other directions because their phase difference is $e^{\pm\pi i/3}$. As a result, the conductance takes a stripe-like pattern consisting or parallel lines in the axis direction.

In Fig. 3 (e), a Kekulé pattern is recovered although weak. In this case, the coupling of the left STM tip to two A sites at $\vec{\tau}_2$ and $\vec{\tau}_3$ is the largest. However, the conductance is not maximum when the right tip is at corresponding A sites related through the basis vectors $\tilde{\boldsymbol{a}}$ and $\tilde{\boldsymbol{b}}$, but maximum at other A sites. This is to be expected because the injection from these two A sites is equivalent to the injection with opposite sign of the wavefunction from the other A site at $\vec{\tau}_1$, as mentioned in §2.

In Fig. 3 (f), the left STM tip is located at the center of a hexagon. Because of the mirror symmetry, electron is injected only into the right–going wave at K' point with $p=1$ and thus the Kekulé pattern disappears. The conductance is the largest at the middle of neighbor carbon atoms along the circumference, due to constructive interference of wavefunctions at these atoms with the same phase. Such strong constructive interference does not occur along $\vec{\tau}_2$ or $\vec{\tau}_3$, where a phase difference is $2\pi/3$ between the nearest–neighbor atoms.

Figure 4 shows the results for varying the position from 'g' to 'l' shown in Fig. 2. As shown in (g), the slight shift of the left tip near the center of the hexagon gives rise to a drastic change in the conductance pattern. This happens due to the variation of interference because the couplings to several carbon atoms are comparable. With the increase in the deviation from the hexagon center, the image varies continuously from (g) to (k). In (k), in particular, the left STM is located above the middle of them $\vec{\tau}_3/2$, where the couplings of the STM tip to two neighbor carbon atoms are the same. In this case, the Kekulé pattern is shown with maximum at translational symmetry position of these two atoms. In (l), while the left tip shifts toward the initial B site, calculated conductance becomes similar to Fig. 3 (a), where the coupling to the B site dominates.

Figure 5 shows the results for the left tip at 'm' and 'n' shown in Fig. 2. With the deviation of the left tip from the B site to the neighboring A site in

the direction $\vec{\tau}_1$, the Kekulé pattern becomes weaker as shown in (m). When the tip is at the middle of the A and B site as in (n), the mirror symmetry is recovered and the conductance is qualitatively the same as Fig. 3 (f) without the Kekulé interference.

§4. Discussions and Conclusions

The numerical results presented in the previous section shows that a Kekulé pattern appears in the conductance of two STM tips due to interference of waves associated with K and K' states. This fact is expected to prevail in all metallic nanotubes other than the armchair type considered here. Further, in special cases where an electron is injected into a single propagating state classified by the parity in the $\boldsymbol{k}\cdot\boldsymbol{p}$ scheme, such interference pattern disappears. This fact is also not limited to armchair nanotubes. In fact, the injection to a single parity state is shown to be possible for arbitrary chirality as discussed in Appendix A.

An actual STM tip usually has a radius larger than the atomic distance and therefore the tunneling process may be much more complicated than discussed in the present model. In fact, the tunneling current injected into a carbon atom of the nanotube is likely to pass through the closest atom on the tip surface. The relevant tip atom can be different for each carbon atom depending on the detailed structure of the STM tip and may even vary with a slight movement of the tip position.

Although the injection into a single parity state is possible even in such a case, the tip position is likely to be different from that obtained above and vary depending of the local atomic structure of the tip. Therefore, a very precise control of the tip position is required for the observation of STM image without a Kekulé pattern resulting from the injection into a single parity state. Further improvement of the spatial resolution in the multi-tip STM measurement may be required for the observation of the appearance and disappearance of interference effects predicted in this paper.

In summary, we have calculated numerically the conductance between two STM probes in an armchair nanotube. The STM probes have been modeled with *sp* Slater–Koster hopping terms. It has been shown that a Kekulé pattern usually appears due to interference between traveling waves at K and K' points. We also find special cases that the Kekulé pattern disappears when the electron wave is injected into a single K or K' point. It is also interesting to study the similar problem in semiconducting nanotubes and in a narrow graphene ribbon. Those are left for a future study.

Acknowledgments

This work was supported in part by a 21st Century COE Program at Tokyo Tech "Nanometer-Scale Quantum Physics" and by Grants-in-Aid for Scientific Research and Scientific Research on Priority Area "Carbon Nanotube Nano-Electronics" from the Ministry of Education, Culture, Sports, Science and Technology, Japan.

Appendix A: Disappearance of Interference

We have shown that the injection into a single parity state is possible in armchair nanotubes in §2. Here we extend our argument to nanotubes with arbitrary chirality. As the simplest example, we consider the case that an STM tip weakly couples with three neighboring carbon atoms. Consider first the right-going wave at the K point $\boldsymbol{F}^{K+}$ with parity $p=-1$ given by eq. (2.5). The wave function at a B site denoted by B_1 with $\boldsymbol{R}_B$ and those at three neighboring A sites denoted by A_l with $\boldsymbol{R}_B+\vec{\tau}_l$ $(l=1,2,3)$ are

$$\begin{aligned}\psi_A(\boldsymbol{R}_B+\vec{\tau}_l) &= \mathrm{e}^{\mathrm{i}\boldsymbol{K}\cdot(\boldsymbol{R}_B+\vec{\tau}_l)}\frac{-\mathrm{i}}{\sqrt{2LA}},\\ \psi_B(\boldsymbol{R}_B) &= -\omega\mathrm{e}^{\mathrm{i}\eta}\mathrm{e}^{\mathrm{i}\boldsymbol{K}\cdot\boldsymbol{R}_B}\frac{1}{\sqrt{2LA}}.\end{aligned} \tag{A1}$$

Therefore, the phases of $\psi_A(\boldsymbol{R}_B+\vec{\tau}_l)$ relative to $\psi_B(\boldsymbol{R}_B)$ are $z_1=\mathrm{i}\mathrm{e}^{-\mathrm{i}\eta}$ for A_1, $z_2=\mathrm{i}\omega\mathrm{e}^{-\mathrm{i}\eta}$ for A_2, and $z_3=\mathrm{i}\omega^{-1}\mathrm{e}^{-\mathrm{i}\eta}$ for A_3. These points are plotted together with $z_0=1$ corresponding to B_1 in a complex plane in Fig. 6 The chiral angle has been chosen in the region $0\le\eta<\pi/6$.

For this choice the triangle consisting of B_1, A_1, and A_2 contains the origin. By moving A_1 to A_1' along the line OA_1 and A_2 to A_2' along OA_2 in appropriate manner, we can construct a triangle $B_1A_1'A_2'$ in such a way that its center-of-mass is at the origin. Let A_1' and A_2' be the distance between the origin and the points A_1' and A_2'. Then, we obviously have

$$\psi_A(\boldsymbol{R}_B+\vec{\tau}_1)A_1'+\psi_A(\boldsymbol{R}_B+\vec{\tau}_2)A_2'+\psi_B(\boldsymbol{R}_B)=0. \tag{A2}$$

At a point satisfying the condition that the coupling to these three sites A_1, A_2, and B_1 corresponds to $A_1'\delta$, $A_2'\delta$, and δ, respectively, with appropriate value of δ, the electron is not injected into $\boldsymbol{F}^{K+}$ but into $\boldsymbol{F}^{K'+}$ only, and therefore no interference pattern appears in the STM image. A similar condition can be written down for the right-going wave $\boldsymbol{F}^{K'+}$ at the K' point and we can find out the position where the electron is not injected into this traveling wave.

References

1) T. Ando and T. Nakanishi, J. Phys. Soc. Jpn. **67** (1998) 1704.
2) T. Ando, T. Nakanishi, and R. Saito, J. Phys. Soc. Jpn. **67** (1998) 2857.
3) T. Nakanishi and T. Ando, J. Phys. Soc. Jpn. **68** (1999) 561.
4) T. Ando and H. Suzuura, J. Phys. Soc. Jpn. **71** (2002) 2753.
5) M. Aono, C.-S. Jiang, T. Nakayama, T. Okuda, S. Qiao, M. Sakurai, C. Thirstrup, and Z.-H. Wu, Oyo Butsuri **67** (1998) 1361 (in Japanese).
6) I. Shiraki, F. Tanabe, R. Hobara, T. Nagao, and S. Hasegawa, Surf. Sci. **493** (2001) 633.
7) H. Watanabe, C. Manabe, T. Shigematsu, and M. Shimizu, Appl. Phys. Lett. **78** (2001) 2928.
8) H. Grube, B. C. Harrison, J.-F. Jia, and J. J. Boland, Rev. Sci. Instrum. **72** (2001) 4388.
9) H. Okamoto and D.-M. Chen, Rev. Sci. Instrum. **72** (2001) 4398.
10) J. Onoe, T. Nakayama, M. Aono, and T. Hara,

Appl. Phys. Lett. **82** (2003) 595.

11) K. Takami, M. Akai-Kasaya, A. Saito, M. Aono, and Y. Kuwahara, Jpn. J. Appl. Phys. **44** (2005) L120.

12) O. Guise, H. Marbach, J. T. Yates, Jr., M.-C. Jung, J. Levy, and J. Ahner, Rev. Sci. Instrum. **76** (2005) 045107.

13) M. Ishikawa, M. Yoshimura, and K. Ueda, Jpn. J. Appl. Phys. **44** (2005) 1502.

14) O. Kubo, Y. Shingaya, M. Nakaya, M. Aono, and T. Nakayama, Appl. Phys. Lett. **88** (2006) 254101.

15) L. C. Venema, J. W. G. Wildoer, J. W. Janssen, S. J. Tans, H. L. J. T. Tuinstra, L. P. Kouwenhoven, and C. Dekker, Science **283** (1999) 52.

16) S. G. Lemay, J. W. Janssen, M. van den Hout, M. Mooij, M. J. Bronikowski, P. A. Willis, R. E. Smalley, L. P. Kouwenhoven, and C. Dekker, Nature **412** (2001) 617.

17) A. Rubio, D. Sanchez-Portal, E. Artacho, P. Ordejon, and J. M. Soler, Phys. Rev. Lett. **82** (1999) 3520.

18) A. Rubio, Appl. Phys. A **68** (1999) 275.

19) V. Meunier and Ph. Lambin, Phys. Rev. Lett. **81** (1998) 5588.

20) Ph. Lambin, G. I. Márk, V. Meunier, L. P. Biró, Int. J. Quantum Chem. **95** (2003) 493.

21) D. Orlikowski, M. B. Nardelli, J. Bernholc, and C. Roland, Phys. Rev. B **61** (2000) 14193.

22) G. I. Márk, L. P. Biró, J. Gyulai, P. A. Thiry, A. A. Lucas, and Ph. Lambin, Phys. Rev. B **62** (2000) 2797.

23) N. Tsuji, S. Takajo, and H. Aoki, Phys. Rev. B **75** (2007) 153406.

24) T. Ando, J. Phys. Soc. Jpn. **74** (2005) 777.

25) M. Igami, T. Nakanishi, and T. Ando, J. Phys. Soc. Jpn. **68** (1999) 716.

26) T. Yaguchi and T. Ando, J. Phys. Soc. Jpn. **70** (2001) 1327.

27) H. Matsumura and T. Ando, J. Phys. Soc. Jpn. **67** (1998) 3542.

28) D. Tomanek and S. G. Louie, Phys. Rev. B **37** (1988) 8327.

Table I The coordinates of the left STM tip shown in Fig. 2 and the maximum values of the conductance, $G_{\max}$, used for plotting Figs. 3, 4, and 5.

	$\sqrt{3}\Delta x/a$	$3\Delta y/a$	$G_{\max}$ $(10^{-10}e^2/\pi\hbar)$
(a)	0	0	9.9
(b)	0.25	0	7.1
(c)	0.5	0	3.2
(d)	0.63	0	1.6
(e)	0.75	0	1.2
(f)	1.0	0	0.24
(g)	0.9	0.1	0.60
(h)	0.8	0.2	1.4
(i)	0.7	0.3	2.4
(j)	0.6	0.4	3.8
(k)	0.25	0.75	6.2
(l)	0.125	0.375	8.1
(m)	−0.25	0	8.3
(n)	−0.5	0	4.2

Figure Captions

Fig. 1 (a) Lattice structure of a two–dimensional graphite sheet. The coordinates are chosen in such a way that x is along the circumference of a nanotube and y is along the axis. η is the chiral angle. (b) A schematic view of a carbon nanotube with two STM tips modeled by 1D wires. (c) A model of the STM tip and the carbon nanotube with a π orbital on a carbon atom at $\boldsymbol{R}$. Δ is the normal distance of the STM tip to the nanotube.

Fig. 2 The left STM-tip positions for which the STM image of the right tip is calculated. The actual coordinates are given in Table I.

Fig. 3 Calculated conductance as a function of right STM tip position for the left-tip position from 'a' to 'f' of Fig. 2. The left STM tip is fixed above a position denoted by a open circle, but its actual position is at $(0, -45)a$ in the coordinate system and therefore is quite far from the right tip. The conductance is shown by the density in the maximum listed in a Table I as plot range.

Fig. 4 Calculated conductance as the function of right STM tip position for the left-tip position from 'g' to 'l' of Fig. 2.

Fig. 5 Calculated conductance as the function of right STM tip position for the left-tip position 'm' and 'n' of Fig. 2.

Fig. 6 The phases of B_1, A_1, A_2, and A_3 of the right-going wave at the K point in a complex plane. The phase of B_1 has been chosen as real and positive. The origin is inside the triangle $B_1A_1A_2$ for $0 \leq \eta < \pi/6$. We can construct the triangle $B_1A_1'A_2'$ with its center-of-mass point at the origin by choosing A_1' on line OA_1 in such a way that C_2 on line A_2O is at the center of $A_1'B_1$ and then A_2' in such a way that C_1 on line A_1O is at the center of $A_2'B_1$.

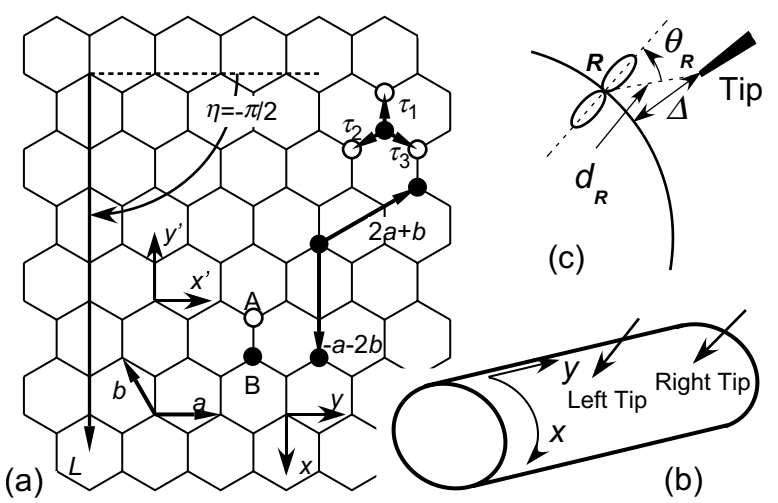

Fig. 1

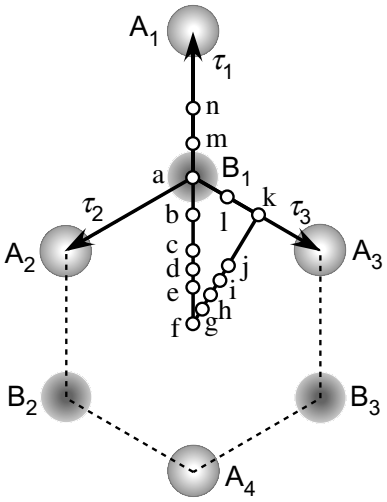

Fig. 2

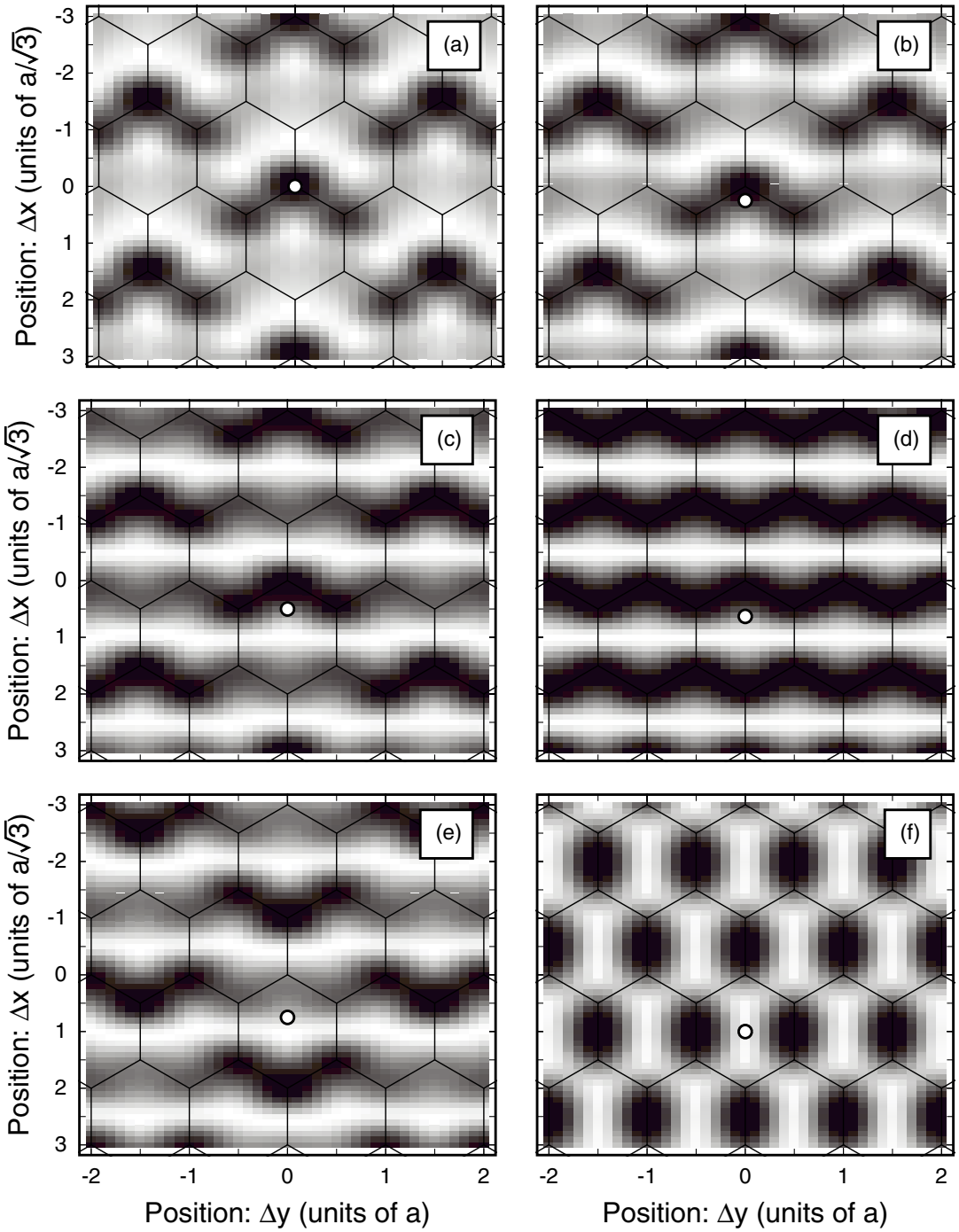

Fig. 3

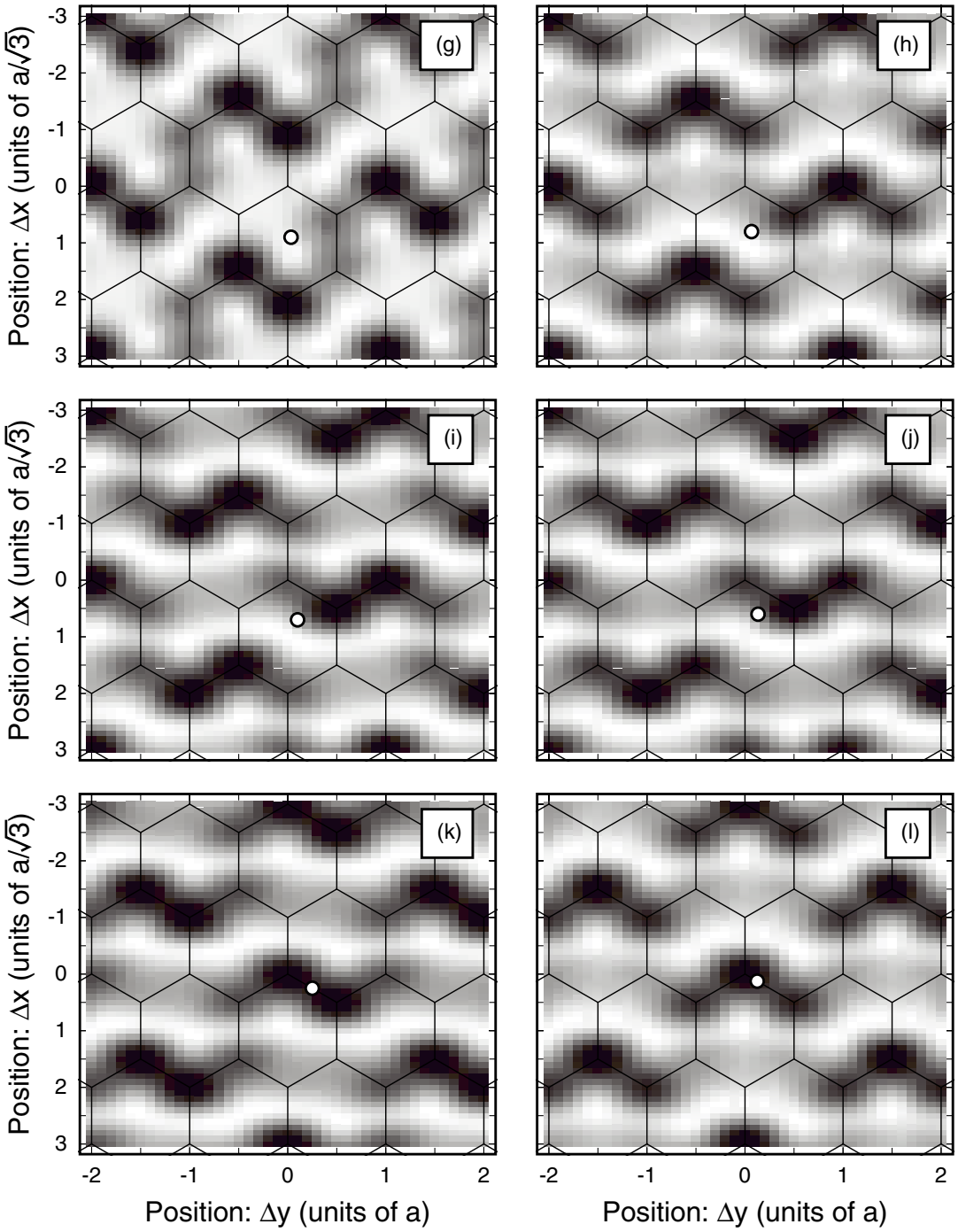
(g)
(h)
(i)
(j)
(k)
(l)
Position: Δx (units of a/√3)
Position: Δy (units of a)
-3
-2
-1
0
1
2
3

Fig. 4

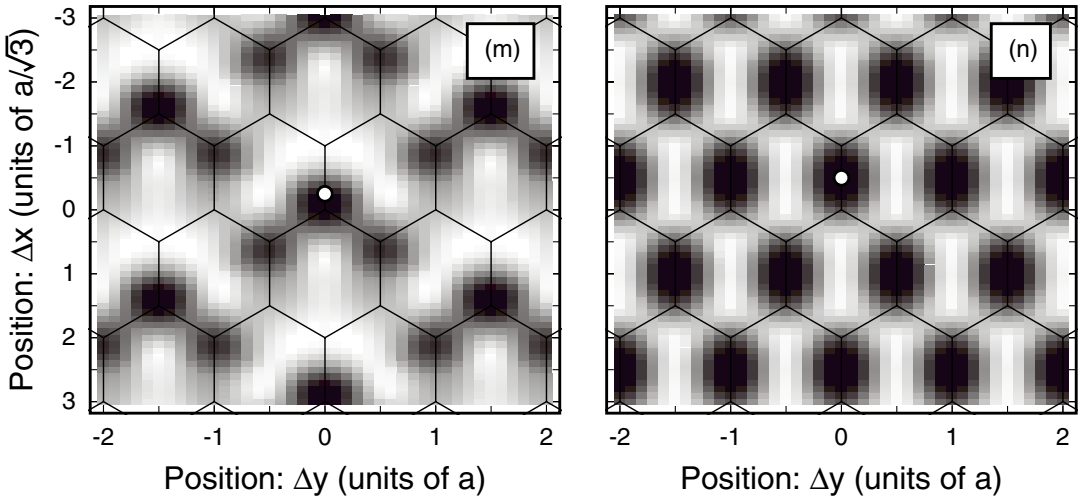
(m)
(n)
Position: Δx (units of a/√3)
Position: Δy (units of a)
-3
-2
-1
0
1
2
3

Fig. 5

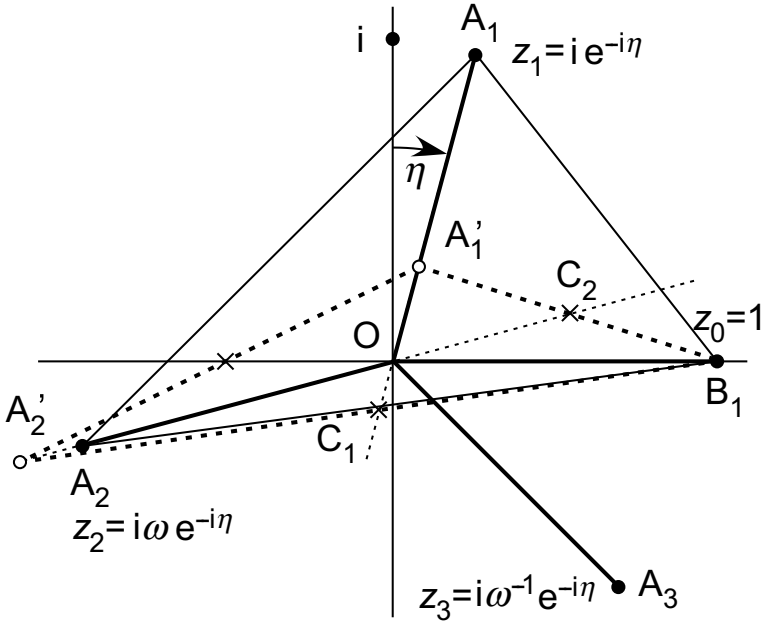

Fig. 6